

Supplement of Biogeosciences, 13, 1597–1607, 2016
<http://www.biogeosciences.net/13/1597/2016/>
doi:10.5194/bg-13-1597-2016-supplement
© Author(s) 2016. CC Attribution 3.0 License.



Supplement of

Climate-driven shifts in continental net primary production implicated as a driver of a recent abrupt increase in the land carbon sink

W. Buermann et al.

Correspondence to: Wolfgang Buermann (w.buermann@leeds.ac.uk)

The copyright of individual parts of the supplement might differ from the CC-BY 3.0 licence.

1 **Supplement**

2

3 **This file includes:**

4

5 **Supplement Figures S1-S6**

6 **Supplement Tables S1-S3**

7 **Supplement Methods**

8 a.) Estimation of Global shifts in NPP, R_h and NEP in the Late 1980s

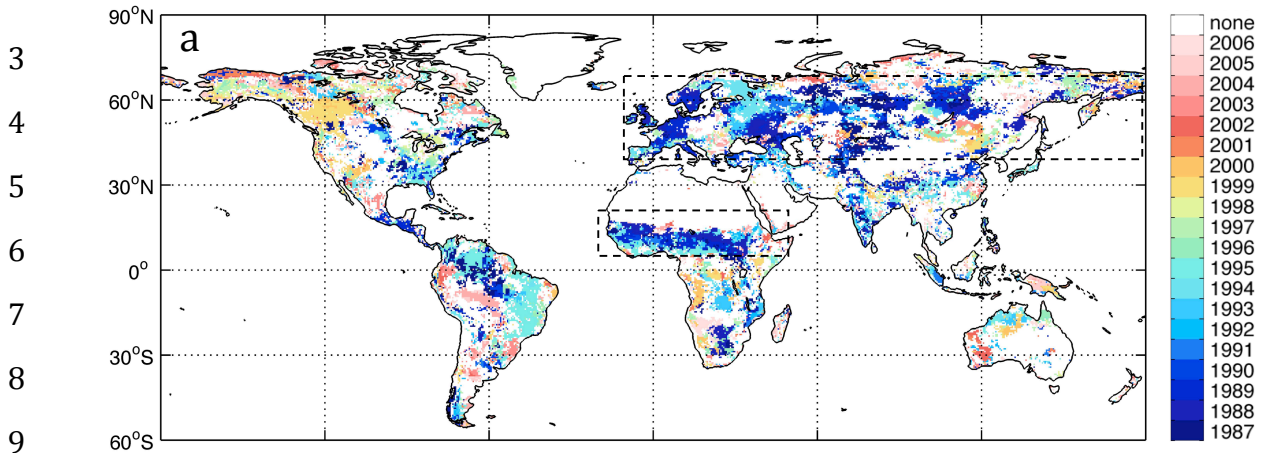
9 b.) Evaluation of Key Driver Datasets for CASA Simulations (Table S4 and Figs S7-S11)

10 **Supplement References**

11

1 Supplement Figures

2



10

11

12

13

14

15

16

17

18 **Figure S1. Spatial pattern of abrupt shifts in data-driven NPP.** Maps show (a) timing and
19 corresponding (b) direction and magnitude of abrupt shifts in data-driven (CASA) annual NPP in
20 the satellite period 1982 to 2011. At each grid-point, three models were fitted including ‘constant
21 mean’, ‘shift in the mean’ and ‘linear trend’ (see Section 2 in manuscript), and regions that are
22 best represented by the ‘shift in the mean’ model are contoured. These results illustrate that for
23 many land regions a ‘shift in the mean’ model fits terrestrial NPP dynamics over the roughly last
24 3 decades better than, for example, a linear trend. Further, many of the local shifts within the two
25 target regions northern Eurasia and northern Africa (dashed rectangles in map (a)) are also
26 statistically significant (see Fig. 1 in manuscript).

27

1
2
3
4
5
6
7
8
9
10
11
12
13
14
15
16
17
18
19

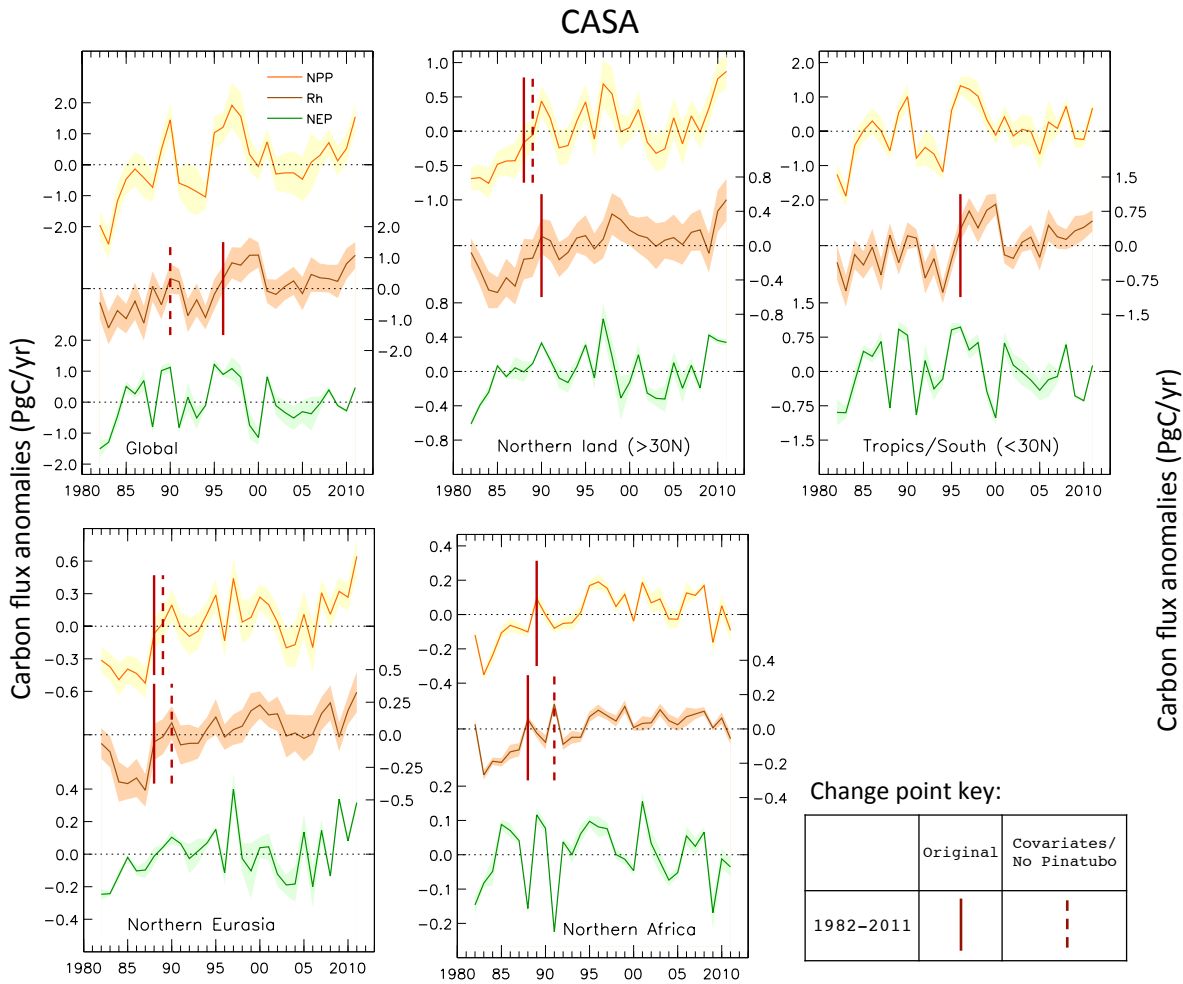


Figure S2 Temporal changes in global and regional carbon fluxes based on CASA. Panels show annual NPP, R_h and NEP anomalies for global land and four focus regions. All anomalies are relative to the satellite 1982-2011 study period. Shaded contours represent 1σ uncertainties that account for biases in model driver data (see Section 2 in manuscript). Statistically significant ($P < 0.05$) ‘shifts in the mean’ in the respective carbon flux time series (see Table 1 in manuscript) are highlighted according to the change point key provided in the figure legend.

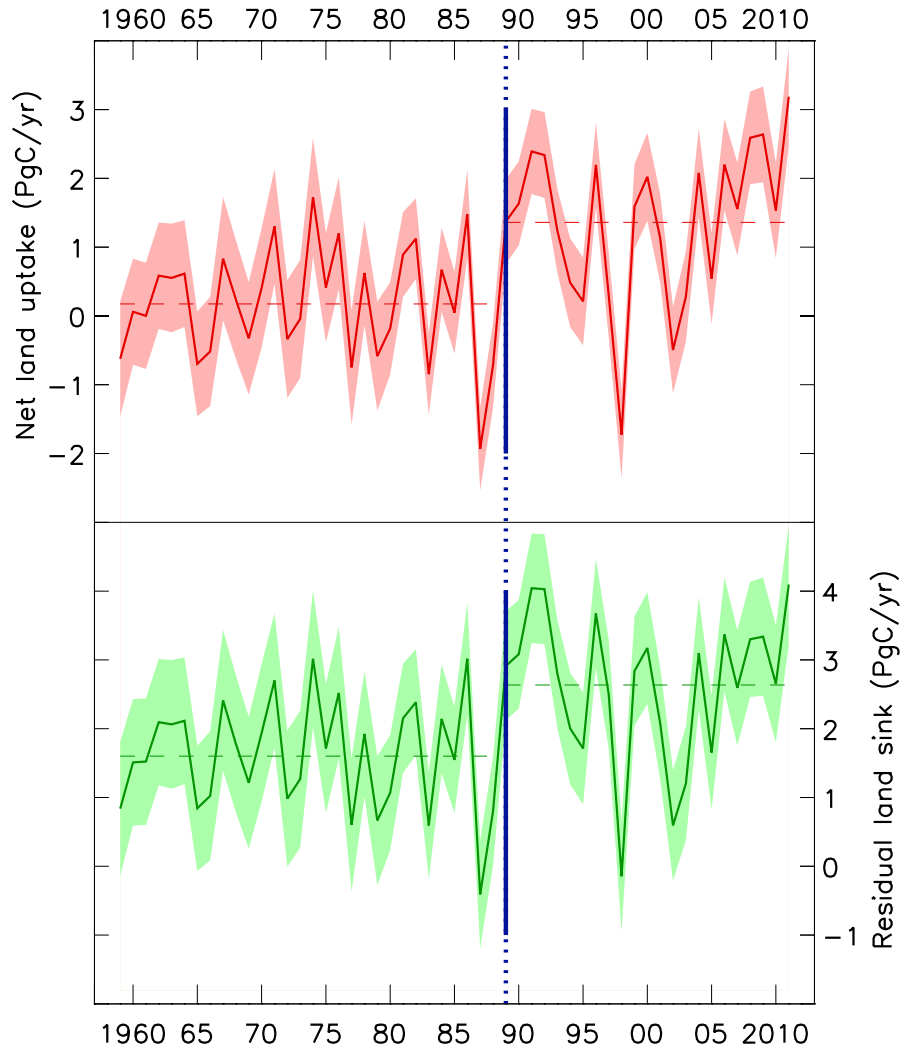


Figure S3. Temporal changes in global land-atmosphere carbon fluxes. Data are from the global carbon budget (Le Quéré et al., 2013; ref. in manuscript), and shaded contours represent 1σ uncertainties. In brief, the net land uptake (red) is inferred as the difference between fossil fuel emissions (estimated through inventories) and the sum of oceanic uptake (inferred through models subject to observational constraints) and atmospheric CO_2 growth rates (based on measurements). The ‘residual’ land sink (green) is then estimated as the difference between net land uptake and net LUC emissions (inferred through a combination of techniques). Change point analysis with explicit accounting for uncertainties (see Section 2 in manuscript) shows that the ‘residual’ land sink and the net land uptake are best represented by a statistical model with a ‘shift in the mean’ in 1989 (thick dark blue lines, see also Table 1 in manuscript). Taken together, these results confirm earlier results based on a less rigorous treatment of uncertainties in the global carbon budget (Beaulieu et al., 2012a; ref. in manuscript).

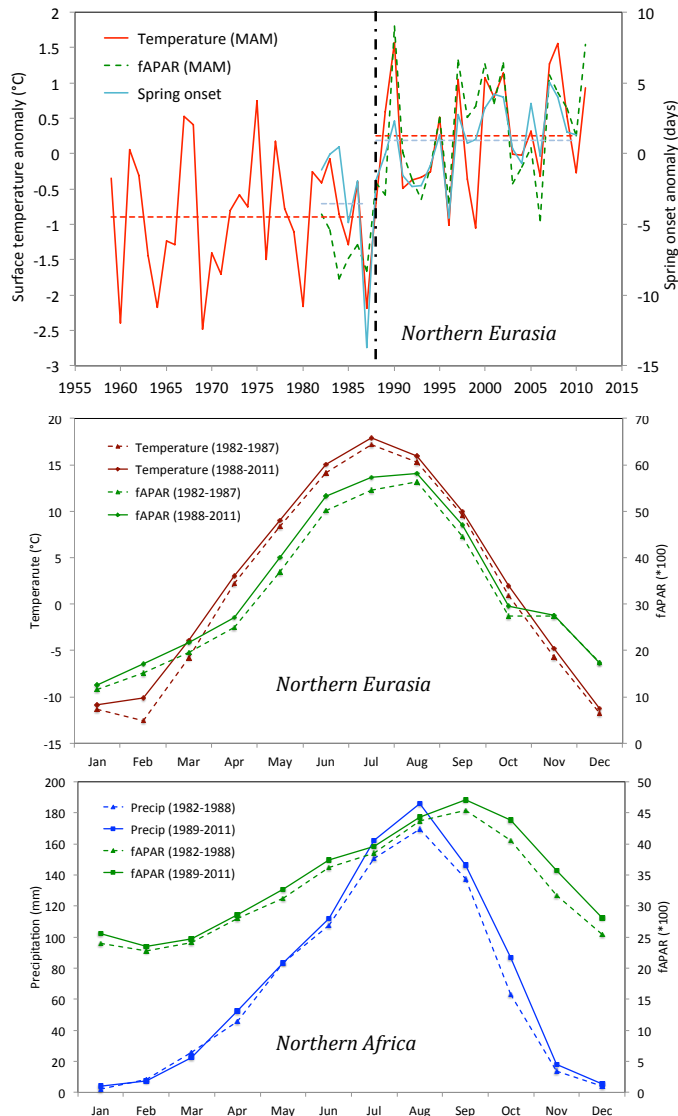


Figure S4. Interannual and seasonal changes in key forcing variables of data-driven NPP for northern Eurasia and northern Africa. Top panel shows spring (MAM) temperature and satellite fAPAR anomalies for the northern Eurasian target region plotted alongside anomalies in timing of spring onset (positive values correspond to earlier onset) representative of the same region and estimated through satellite microwave freeze-thaw data available for the period 1982-2010 (Kim et al., 2012). All anomalies are relative to 1982-2010. fAPAR data are scaled to allow visual comparisons. For the northern Eurasian region, interannual variations in the timing of spring onset as well as spring temperature and fAPAR are tightly coupled. Correlations between timing of spring onset and spring temperatures are $r=0.84$ ($P<0.001$), for timing of spring onset and spring fAPAR $r=0.72$ ($P<0.001$), and for spring temperatures and spring fAPAR $r=0.79$ ($P<0.001$), respectively. The drastic change in spring temperatures that accompanied the identified late 1980s NPP shift (see Table 1 in ms) is of the order of 1.2°C , whereas the timing of spring onset occurred about 5 days earlier in the period after the shift (dashed lines). The middle panel shows the seasonal cycles of satellite fAPAR and temperature representative of northern Eurasia for the periods prior and after the ‘1988’ shift, whereas the bottom panel shows the seasonal cycles of fAPAR and precipitation representative for northern Africa for the periods prior and after the ‘1989’ shift (see also Table 1 in manuscript).

1
2
3
4
5
6
7
8
9
10
11
12
13
14
15
16
17
18
19
20
21
22
23
24

TRENDY - Climate varied only (S2 –S1)

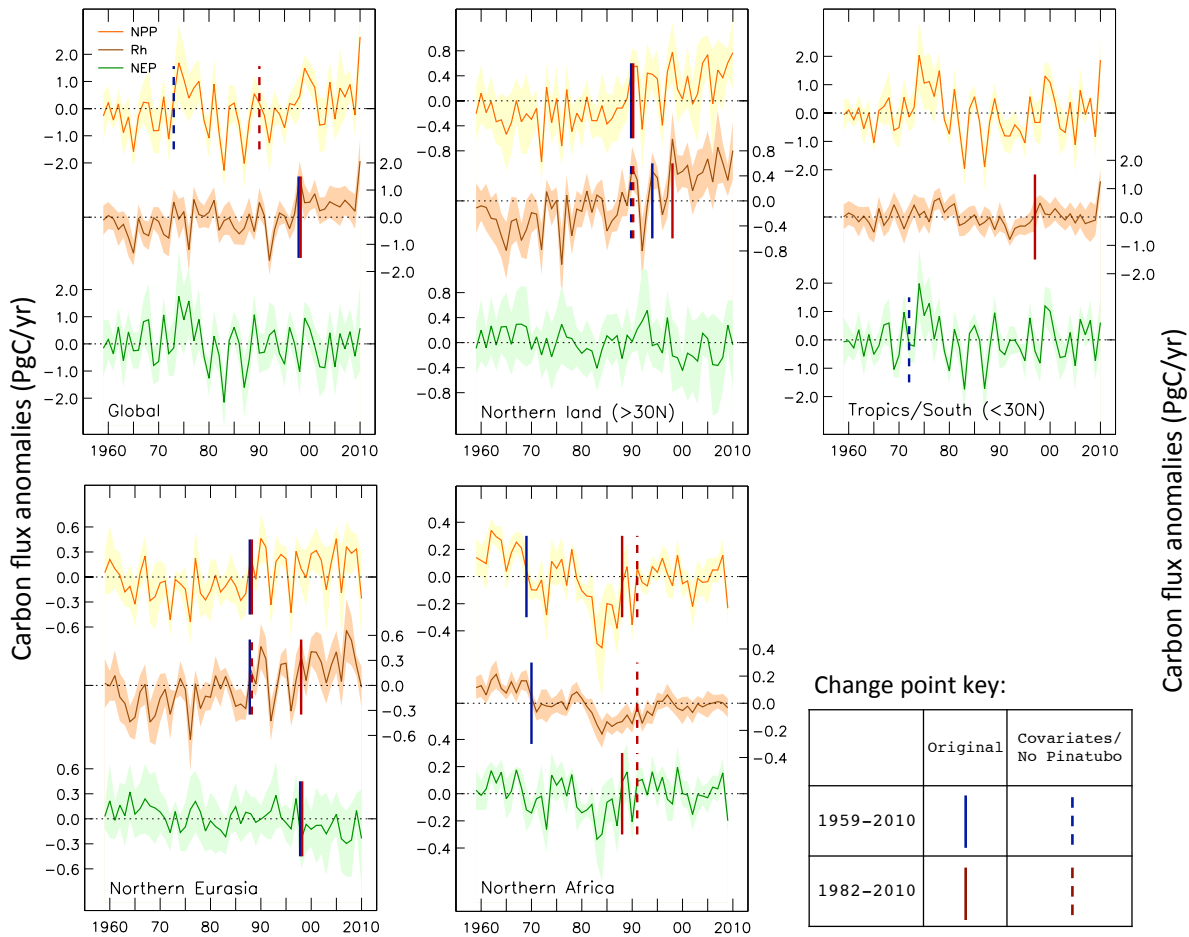


Figure S5. Temporal changes in global and regional carbon fluxes based on the TRENDY experiments with climate varied only (S2 – S1). Panels show annual NPP, R_h and NEP anomalies for global land and four focus regions, based on ensembles of eight biosphere models (no Orchidee simulations were available for extended study period) that participated in the recent TRENDY model intercomparison study (Sitch et al. 2015). All anomalies are relative to the extended 1959-2010 study period. Mean ensembles were formed based on anomalies in the single TRENDY models to emphasize temporal changes in NPP and to suppress uncertainties arising from model differences in magnitudes. Shaded contours represent 1σ uncertainties corresponding to the spread in the single TRENDY models. Statistically significant ($P < 0.05$) ‘shifts in the mean’ in the respective carbon flux time series (see Table S1-S3) are highlighted according to the change point key provided in the figure legend.

1
2
3
4
5
6
7
8
9
10
11
12
13
14
15
16
17
18
19
20
21
22
23
24

TRENDY – CO2 and Climate varied (S2)

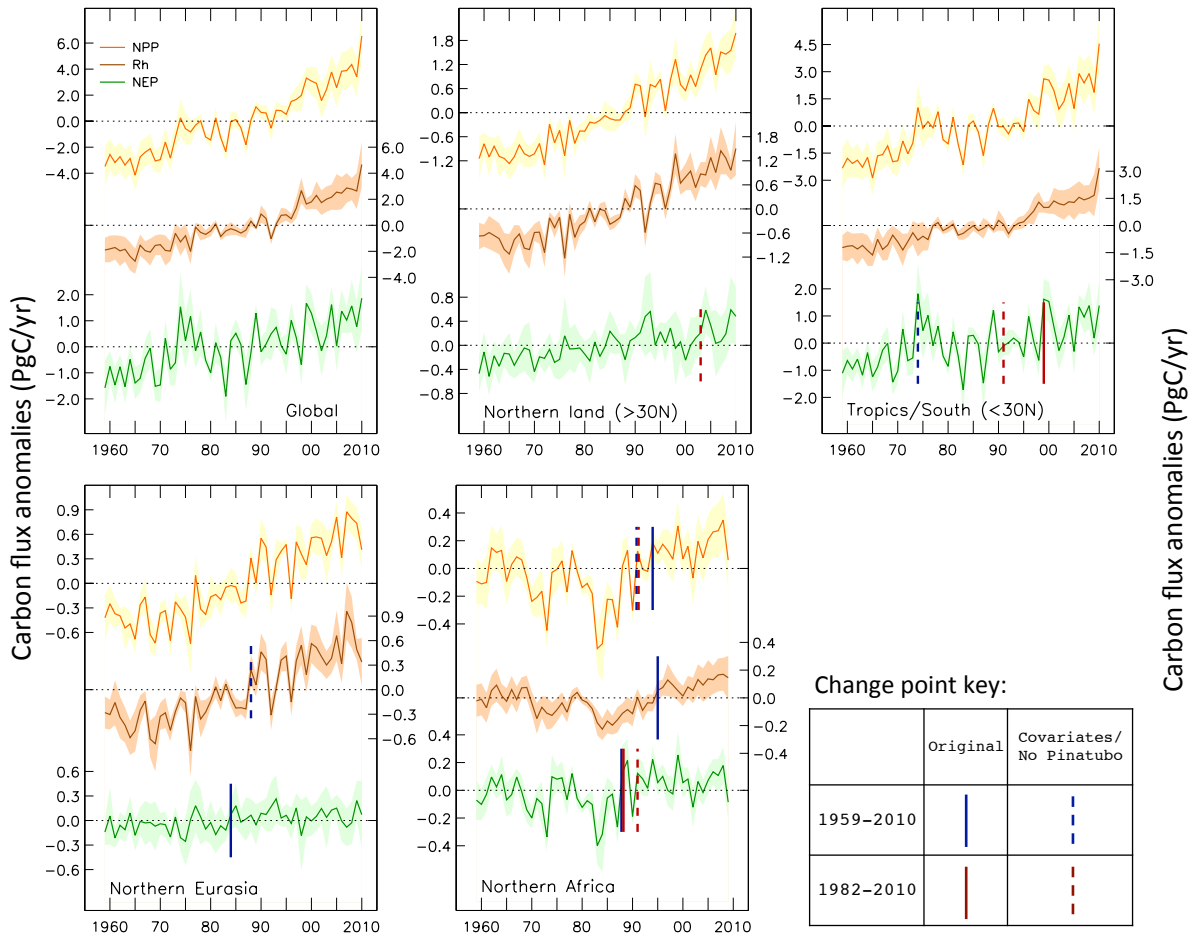


Figure S6. Temporal changes in global and regional carbon fluxes based on the TRENDY experiments with CO₂ and Climate varied (S2). Panels show annual NPP, R_h and NEP anomalies for global land and four focus regions, based on ensembles of eight biosphere models (no Orchidee simulations were available for extended study period) that participated in the recent TRENDY model intercomparison study (Sitch et al. 2015). All anomalies are relative to the extended 1959-2010 study period. Mean ensembles were formed based on anomalies in the single TRENDY models to emphasize temporal changes in NPP and to suppress uncertainties arising from model differences in magnitudes. Shaded contours represent 1σ uncertainties corresponding to the spread in the single TRENDY models. Statistically significant ($P < 0.05$) ‘shifts in the mean’ in the respective carbon flux time series (see Table S1-S3) are highlighted according to the change point key provided in the figure legend.

1 Supplement Tables

2 **Table S1. Timing and magnitude of abrupt changes in global and continental process-based**
 3 **NPP data, based on the TRENDY model ensembles.** Results are for ensembles based on 9
 4 models of the terrestrial biosphere that participated in TRENDY and experiments in which
 5 climate and CO₂ driver data (S2) as well as climate driver data only (S2 – S1) were varied (see
 6 also Section 2 in ms). Shown are timing of the most likely shift (first data entry) along with
 7 associate direction and magnitude (second data entry in units of PgC yr⁻¹) and *P*-value (in
 8 brackets). Magnitude and *P*-values are only provided if the ‘shift in the mean model’ was more
 9 likely than a ‘linear trend’ or ‘constant mean’ model. The timing of a shift captures the first year
 10 of a new regime. The *P*-values are obtained using Monte Carlo simulations that take into account
 11 uncertainty in the original data. Bold indicates shifts that are significant at the 5% critical level.

Region	Experiment	Original data	Covariates ^c	No Pinatubo ^f
<i>Process-based (TRENDY) NPP 1982-2010</i>				
Global	S2 – S1	1996 ^d	1990, +0.81 (0.016)	1989 ^d
	S2	1997 ^d	1997 ^d	1996 ^d
North (>30°N)	S2 – S1	1990, +0.51 (0.001)^b	1989, +0.50 (0.002)	1990, +0.53 (0.004)^b
	S2	1997 ^d	1990 ^d	1990 ^d
Tropics/South (<30°N)	S2 – S1	1996, +0.76 (0.061)	1996, +0.52 (0.087)	1996, +0.76 (0.112)
	S2	1996 ^d	1996 ^d	1996 ^d
Northern Eurasia	S2 – S1	1988, +0.26 (0.004)^a	1988, +0.26 (0.098)	1988, +0.28 (0.003)^a
	S2	1990 ^d	1990 ^d	1990 ^d
Northern Africa	S2 – S1	1988, +0.27 (0.001)	1991, +0.30 (0.003)^a	1988 +0.30 (<0.001)^a
	S2	1988 ^d	1991, +0.44 (<0.001)	1991 ^d
<i>Process-based (TRENDY) NPP 1959-2010^g</i>				
Global	S2 – S1	1998, +0.79 (0.109)	1973, +0.75 (0.019)^{b,c}	1998, +0.77 (0.138)
	S2	1996 ^d	1989 ^d	1989 ^d
North (>30°N)	S2 – S1	1990, +0.55 (<0.001)	1990, +0.54 (<0.001)	1990, +0.59 (<0.001)
	S2	1990 ^d	1990 ^d	1990 ^d
Tropics/South (<30°N)	S2 – S1	1979 ^d	1972, +0.51 (0.163)	1979 ^e
	S2	1996 ^d	1991 ^d	1996 ^d
Northern Eurasia	S2 – S1	1988, +0.25 (<0.001)	1988, +0.24 (0.001)	1988, +0.27 (<0.001)
	S2	1988 ^d	1988 ^d	1988 ^d
Northern Africa	S2 – S1	1969, -0.24 (0.038)^{b,c}	1970, -0.21 (0.077) ^{b,c}	1969 -0.24 (0.044)^{b,c}
	S2	1994, +0.30 (<0.001)^c	1991, +0.32 (<0.001)^c	1991, +0.31 (0.001)^c

12 a. Not normally distributed (Lilliefors test, 5% critical level); b. Variance not constant (F-test, 5% critical level)
 13 c. Residuals not independent (Kruskal-Wallis, 5% critical level); d. ‘Linear trend’ or ‘constant mean’ model fits
 14 data better than a ‘shift in the mean’ model; e. Variability related to ENSO and volcanoes were removed in the
 15 original time series through regressions against the multivariate ENSO index and stratospheric optical thickness after
 16 Beaulieu et al. (2012a, ref. in manuscript); f. The two Pinatubo years (1992, 1993) were removed in the original
 17 time series prior change point analysis; g. For period 1959-2010, TRENDY ensembles are based on 8 models only
 18 (no Orchidee simulations available for extended period)

19

1 **Table S2. Timing and magnitude of abrupt changes in global and continental process-based**
2 **R_h data, based on the TRENDY model ensembles.** Results are for ensembles based on 9
3 models of the terrestrial biosphere that participated in TRENDY and experiments in which
4 climate and CO₂ driver data (S2) as well as climate driver data only (S2 – S1) were varied (see
5 also Section 2 in ms). Shown are timing of the most likely shift (first data entry) along with
6 associate direction and magnitude (second data entry in units of PgC yr⁻¹) and *P*-value (in
7 brackets). Magnitude and *P*-values are only provided if the ‘shift in the mean model’ was more
8 likely than a ‘linear trend’ or ‘constant mean’ model. The timing of a shift captures the first year
9 of a new regime. The *P*-values are obtained using Monte Carlo simulations that take into account
10 uncertainty in the original data. Bold indicates shifts that are significant at the 5% critical level.

Region	Experiment	Original data	Covariates ^c	No Pinatubo ^f
<i>Process-based (TRENDY) R_h 1982-2010</i>				
Global	S2 – S1	1998, +0.90 (<0.001)	1998, +0.69 (0.005)	1998, +0.80 (<0.001)
	S2	1997 ^d	1997 ^d	1997 ^d
North (>30°N)	S2 – S1	1998, +0.53 (0.001)	1998, +0.44 (0.026)	1990, +0.56 (<0.001)
	S2	1998 ^d	1998 ^d	1998 ^d
Tropics/South (<30°N)	S2 – S1	1997, +0.39 (0.021)^{a,b}	1997, +0.26 (0.258) ^b	1997, +0.33 (0.039)^{a,b}
	S2	1997 ^d	1997 ^d	1997 ^d
Northern Eurasia	S2 – S1	1998, +0.25 (0.084)	1990, +0.22 (0.214)	1988, +0.34 (0.037)
	S2	1997 ^d	1990 ^d	1990 ^d
Northern Africa	S2 – S1	1995 ^d	1991, +0.13 (<0.001)^a	1991, +0.15 (<0.001)^a
	S2	1995 ^d	1991 ^d	1995 ^d
<i>Process-based (TRENDY) R_h 1959-2010^g</i>				
Global	S2 – S1	1998, +0.89 (<0.001)	1998, +0.70 (<0.001)	1998, +0.85 (<0.001)
	S2	1994 ^d	1990 ^d	1990 ^d
North (>30°N)	S2 – S1	1994, +0.68 (<0.001)	1990, +0.60 (<0.001)^a	1990, +0.70 (<0.001)
	S2	1988 ^d	1990 ^d	1988 ^d
Tropics/South (<30°N)	S2 – S1	1982 ^d	1986, -0.19 (0.261)	1998 ^d
	S2	1996 ^d	1996 ^d	1996 ^d
Northern Eurasia	S2 – S1	1988, +0.34 (<0.001)	1988, +0.32 (0.001)	1988, +0.38 (<0.001)
	S2	1988 ^d	1988 ^d	1988, +0.70 (<0.001)
Northern Africa	S2 – S1	1970, -0.17 (0.007)^{a,c}	1970, -0.17 (0.001)^{a,c}	1970, -0.16 (0.004)^{a,c}
	S2	1995, +0.18 (0.006)^c	1995, +0.18 (0.006)^c	1995, +0.18 (0.004)^c

11 a. Not normally distributed (Lilliefors test, 5% critical level); b. Variance not constant (F-test, 5% critical level)
12 c. Residuals not independent (Kruskal-Wallis, 5% critical level); d. ‘Linear trend’ or ‘constant mean’ model fits
13 data better than a ‘shift in the mean’ model; e. Variability related to ENSO and volcanoes were removed in the
14 original time series through regressions against the multivariate ENSO index and stratospheric optical thickness after
15 Beaulieu et al. (2012a, ref. in manuscript); f. The two Pinatubo years (1992, 1993) were removed in the original
16 time series prior change point analysis; g. For period 1959-2010, TRENDY ensembles are based on 8 models only
17 (no Orchidee simulations available for extended period)
18

1 **Table S3. Timing and magnitude of abrupt changes in global and continental process-based**
2 **NEP data, based on the TRENDY model ensembles.** Results are for ensembles based on 9
3 models of the terrestrial biosphere that participated in TRENDY and experiments in which
4 climate and CO₂ driver data (S2) as well as climate driver data only (S2 – S1) were varied (see
5 also Section 2 in ms). Shown are timing of the most likely shift (first data entry) along with
6 associate direction and magnitude (second data entry in units of PgC yr⁻¹) and *P*-value (in
7 brackets). Magnitude and *P*-values are only provided if the ‘shift in the mean model’ was more
8 likely than a ‘linear trend’ or ‘constant mean’ model. The timing of a shift captures the first year
9 of a new regime. The *P*-values are obtained using Monte Carlo simulations that take into account
10 uncertainty in the original data. Bold indicates shifts that are significant at the 5% critical level.

Region	Experiment	Original data	Covariates ^c	No Pinatubo ^f
<i>Process-based (TRENDY) NEP 1982-2010</i>				
Global	S2 – S1	1989 ^d	1989, +0.48 (0.145)	1989 ^d
	S2	1999 ^d	1989 ^d	1999 ^d
North (>30°N)	S2 – S1	1998, -0.22 (0.225)	1998 ^d	1998, -0.16 (0.283)
	S2	2003, +0.22 (0.284)	2003 ^d	2003, +0.27 (0.018)
Tropics/South (<30°N)	S2 – S1	1999 ^d	1989 ^d	1999 ^d
	S2	1999, +0.93 (0.005)	1991, +0.69 (<0.001)	1999, +0.97 (0.008)
Northern Eurasia	S2 – S1	1998, -0.16 (0.015)	1998, -0.16 (0.058)	1998, -0.14 (0.027)
	S2	1990 ^d	2001 ^d	2001 ^d
Northern Africa	S2 – S1	1988, +0.22 (0.002)	1991, +0.16 (0.023)	1988, +0.22 (0.001)
	S2	1988, +0.28 (<0.001)	1991, +0.20 (0.006)	1988, +0.29 (0.001)
----- <i>Process-based (TRENDY) NEP 1959-2010^g</i>				
Global	S2 – S1	1979, -0.46 (0.225)	1974 ^d	1979, -0.50 (0.154)
	S2	1974 ^d	1974 ^d	1974 ^d
North (>30°N)	S2 – S1	1998, -0.21 (0.069)	1979, -0.16 (0.144)	1970, -0.21 (0.052)
	S2	1985 ^d	1985 ^d	1985 ^d
Tropics/South (<30°N)	S2 – S1	1979 ^d	1972, +0.49 (0.030)	1979 ^d
	S2	1971 ^d	1974, +1.29 (<0.001)	1999 ^d
Northern Eurasia	S2 – S1	1998, -0.18 (0.005)	1998, -0.17 (0.018)	1971 ^d
	S2	1984, +0.13 (0.001)	1984, +0.13 (<0.001)	1984, +0.11 (<0.001)
Northern Africa	S2 – S1	1988 ^d	1991, +0.10 (0.070)	1969 ^d
	S2	1988, +0.15 (0.004)	1988, +0.17 (<0.001)^a	1988, +0.15 (0.007)^a

11 a. Not normally distributed (Lilliefors test, 5% critical level); b. Variance not constant (F-test, 5% critical level)
12 c. Residuals not independent (Kruskal-Wallis, 5% critical level); d. ‘Linear trend’ or ‘constant mean’ model fits
13 data better than a ‘shift in the mean’ model; e. Variability related to ENSO and volcanoes were removed in the
14 original time series through regressions against the multivariate ENSO index and stratospheric optical thickness after
15 Beaulieu et al. (2012a, ref. in manuscript); f. The two Pinatubo years (1992, 1993) were removed in the original
16 time series prior change point analysis; g. For period 1959-2010, TRENDY ensembles are based on 8 models only
17 (no Orchidee simulations available for extended period)

1 Supplement Methods

2 a.) Estimation of global shifts in NPP, R_h and NEP in the late 1980s

3 All data for the calculations shown below stem from Table 1 in the main manuscript as well as
4 from Table S1 and S3 and calculations are based on the equation $NEP = NPP - R_h$.

5

6 *Step 1: Estimating shifts in global R_h in the late 1980s using 3 methods*

7 1. Residual (*No Pinatubo*): $R_h \text{ shift} = 1.49 (NPP_{CASA}) - 1.06 (RSL_{GCB}^*) = \underline{0.43 \text{ PgC/yr}}$

8 2. Residual (*Covariates*): $R_h \text{ shift} = 1.12 (NPP_{CASA}) - 1.28 (RSL_{GCB}^*) = \underline{-0.16 \text{ PgC/yr}}$

9 3. Direct: CASA (*Covariates*): $R_h \text{ shift} = \underline{0.80 \text{ PgC/yr}}$

10 * RSL_{GCB} : Residual land sink from the Global Carbon Budget

11

12 *Step 2: Estimating late 1980s NPP as well as corresponding R_h and NEP shifts at global levels*

13 **Global NPP shift:** Mean of 1.12 ($NPP_{CASA-Covariates}$), 1.49 ($NPP_{CASA-No \text{ Pinatubo}}$) and

14 0.81 ($NPP_{TRENDY (S2-S1)-Covariates}$) = **$1.14 \pm 0.34 \text{ PgC/yr}$**

15

16 **Global R_h shift:** Mean of (0.43, -0.16, 0.80; *see Step 1*) = **$0.36 \pm 0.48 \text{ PgC/yr}$**

17

18 Global NEP shift estimated as Global NPP shift – Global R_h shift = $1.14 \pm 0.34 - 0.36 \pm 0.48$

19 yields = $0.78 \pm 0.35 \text{ PgC/yr}$

20

21 **Global NEP shift:** Mean of 0.78 ± 0.35 (from prior step) and 0.48 ($NEP_{TRENDY (S2-S1)-Covariates}$)

22 = **$0.63 \pm 0.35 \text{ PgC/yr}$**

23

1 b.) Evaluation of Key Driver Datasets for CASA Simulations

2 The CASA model is forced by temporally varying estimates of fAPAR, near surface air
3 temperature, precipitation and incoming surface solar radiation at monthly time steps at a spatial
4 resolution of 0.5°. While high-resolution gridded temperature data (CRU TS3.21) are considered
5 relatively robust, uncertainties in global fAPAR, precipitation and solar radiation datasets are
6 potentially large and need to be accounted for in the model simulations. For our study period
7 1981-2011 available data for satellite-based fAPAR are limited to one dataset (FPAR3g; see
8 manuscript). For precipitation and solar radiation multiple datasets exist, and we evaluated a set
9 of candidate datasets (Table S4). The ISCCP solar radiation dataset was removed from further
10 consideration because it was found to be biased high over the Amazon (see below). All
11 combinations of the remaining three solar radiation and three precipitation datasets (Table S4)
12 were used to force the CASA model to produce an ensemble of nine simulations.

13

14 ***Surface Shortwave Radiation***

15 We analyzed three satellite remote sensing and one empirically based estimate of global surface
16 incoming shortwave radiation (Table S4). The satellite-based datasets extend from 1983-2007 as
17 limited by the availability of satellite cloud data and here we use the full years of data (1984-
18 2007). The empirical dataset (Sheffield et al., 2006), which is available for the full time period, is
19 also used to extend the satellite-based datasets to 1982-2011 using pdf matching. All datasets are
20 available at 3-hour resolution and are averaged to monthly means to force the CASA model.

21

1 **Table S4. Surface downward solar radiation and precipitation datasets.**

Dataset	Time period	Domain	Source	Reference
Solar Radiation				
ISCCP FD-SRF*	1984-2007	Global, 280km	Satellite	Zhang et al. (2004)
SRB V3	1984-2007	Global, 1.0deg	Satellite	Stackhouse et al. (2011)
UMD	1983-2007	Global, 0.5deg	Satellite	Mao and Pinker (2012)
PGF	1948-2011	Global, 1.0deg	Empirical (cloud cover)	Sheffield et al. (2006)
Precipitation				
CRU TS3.2	1901-2013	Global, 0.5-deg	Station	Harris et al. (2014)
UDeI V3.01	1900-2010	Global, 0.5-deg	Station	Willmott and Matsuura (2012)
GPCP V2.2	1979-2012	Global, 2.5-deg	Satellite/station	Huffman et al. (2009)

2 *Not included in CASA simulations

3
4

5 *i) International Satellite Cloud Climatology Project (ISCCP)*

6 The ISCCP FD-SRF surface solar radiation flux data are calculated using the NASA Goddard
7 Institute for Space Studies (GISS) radiation transfer model based on ISCCP satellite visible and
8 infrared radiances and cloud properties, and the TIROS Operational Vertical Sounder (TOVS)
9 atmospheric temperature and humidity profiles. The ISCCP cloud data are sampled from multiple
10 geostationary and polar orbiting sensor retrievals which have reasonable spatial and temporal
11 sampling for clear and cloudy conditions, but may suffer from inconsistencies in time due to
12 changes in sensor view angles (Evan et al., 2007).

13
14

1 *ii) Surface Radiation Budget (SRB)*

2 The current version (V3) of the SRB includes estimates of surface radiation components
3 available at 3-hourly and 1.0 degree (~100km) resolution for 1983-2007. The SRB data have
4 explicit representations of aerosols, including dust and black carbon, which, although there
5 remain considerable uncertainties in their distribution and effects, are important factors in
6 regional climate and its terrestrial impacts via changes in available radiation. The fluxes are
7 computed with two retrieval algorithms: a ‘primary’ (SRB) and ‘quality-check’ (SRBqc) and we
8 use the SRB dataset here. The retrievals use temperature and water vapor profiles from the
9 Goddard Earth Observing System (GEOS-4) (Bloom et al., 2005) and satellite visible and
10 infrared radiances and cloud properties from the ISCCP pixel level (DX) data.

11

12 *iii) University of Maryland (UMD)*

13 The UMD dataset of Ma and Pinker (2012) is a relatively new global dataset of surface fluxes at
14 0.5-degree, 3-hourly resolution for 1983 to 2007. These have been generated with V3.3.3 of the
15 UMD/SRB model using ISCCP DX satellite cloud data. This upgrades the previous version of
16 the UMD/SRB model by incorporating new auxiliary information for land cover, improved
17 aerosol treatment and separation of clouds by phase.

18

19 *iv) Princeton Global Forcings (PGF)*

20 The empirical dataset of Sheffield et al. (2006) is based on regressions between monthly
21 downward surface solar radiation and cloud cover developed from the NCEP/NCAR reanalysis
22 (Kalnay et al., 1996) and applied to the observational gridded cloud cover analysis from the CRU
23 TS3.1 dataset (Harris et al. 2014). The values are then scaled to match the climatological values

1 of the UMD dataset. The dataset does not include the direct effect of aerosols and is subject to
2 the uncertainties in the regression relationships and the reliability of the CRU cloud data (Harris
3 et al., 2014). The latter are based on station cloud observations taken from the CRU TS2.0
4 dataset up to 2002, and then derived using relationships with diurnal temperature range
5 thereafter.

6

7 *v) Comparison of solar radiation datasets and evaluation against GEBA station observations*

8 Figures S7-S8 compare the four solar radiation datasets against station observations from the
9 Global Energy Balance Archive (GEBA; Gilgen and Ohmura, 1999). The GEBA contains
10 monthly mean surface radiation flux data for several thousand stations worldwide, with some
11 station records back to 1922. We compare the data for the period 1984-2007 and when GEBA
12 data have more than 10 years of data over this period. Under this criterion, data for 510 GEBA
13 stations are available, which are mainly located in western Europe and east Asia with very few
14 stations over the focus regions of this study. The dataset biases tend to be positive relative to the
15 GEBA stations with the largest biases of the order of 20-50 W/m² over east Asia and northern
16 South America/Caribbean (Figure S7). Correlations between gridded solar radiation and station
17 data (Figure S8) are calculated on the monthly anomalies to remove the seasonal cycle. The
18 correlations are mostly higher than 0.5 and are largest in western Europe and some stations in N.
19 America, east Asia and Australia, with correlations > 0.9. The mean correlation across stations is
20 similar for the satellite based datasets but slightly lower for the empirical dataset (mean
21 correlation: ISCCP = 0.70; SRB = 0.69; UMD = 0.71; PGFemp = 0.59) likely because the
22 empirical dataset does not include direct aerosol effects. The correlations are lowest (< 0.4) at
23 isolated stations across the world, and for nearly all stations in northern South America.

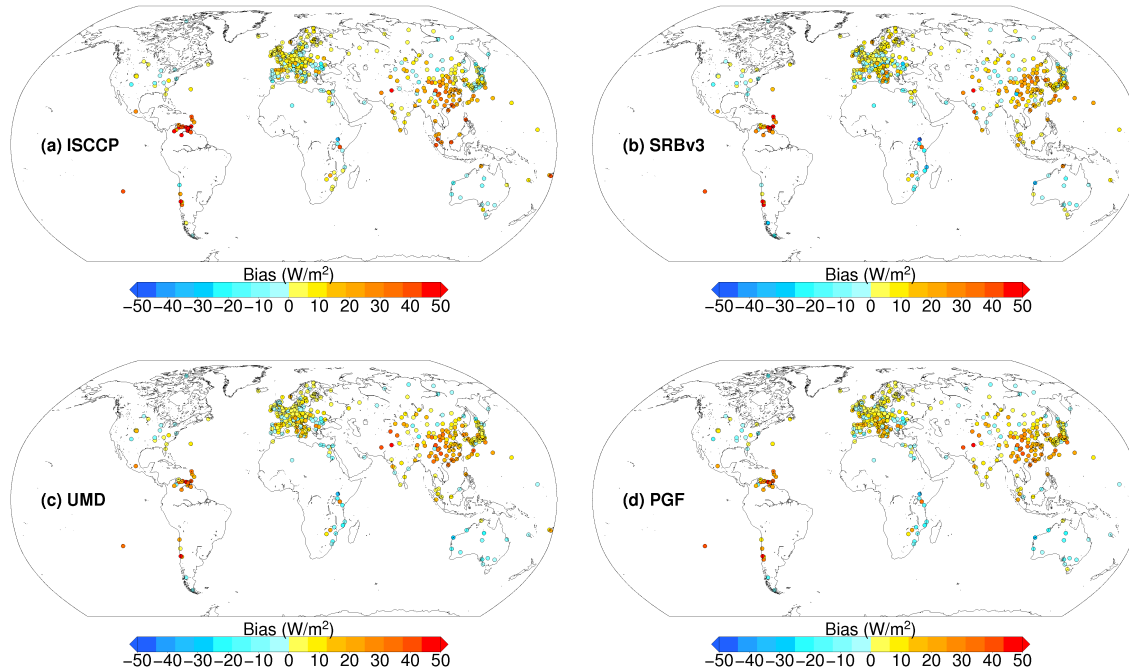
1 Figure S9 shows the annual and monthly times series of solar radiation for the four
2 datasets averaged over the two focus regions northern Eurasia and northern Africa. These regions
3 have very few GEBA stations with available data for our time period and so a comprehensive
4 evaluation against observations is not possible. The data are reasonably well matched in terms of
5 the absolute values and the correlation over time, although there are several aspects of
6 disagreement. The ISCCP and SRB datasets are well correlated over the three regions, but the
7 UMD and PGFemp datasets tend to diverge, especially in the last 10 years. Complementary
8 analysis shows that across the Amazon, the ISCCP dataset is about 15 W/m^2 higher than the
9 other datasets (results not shown), which are likely biased high based on the few GEBA
10 comparisons in the far northern part of South America (Figure S7). Because of this and the fact
11 that the ISCCP dataset are well correlated with the SRB data (and hence does not provide
12 independent information) we did not use the ISCCP data in the CASA simulations.

13

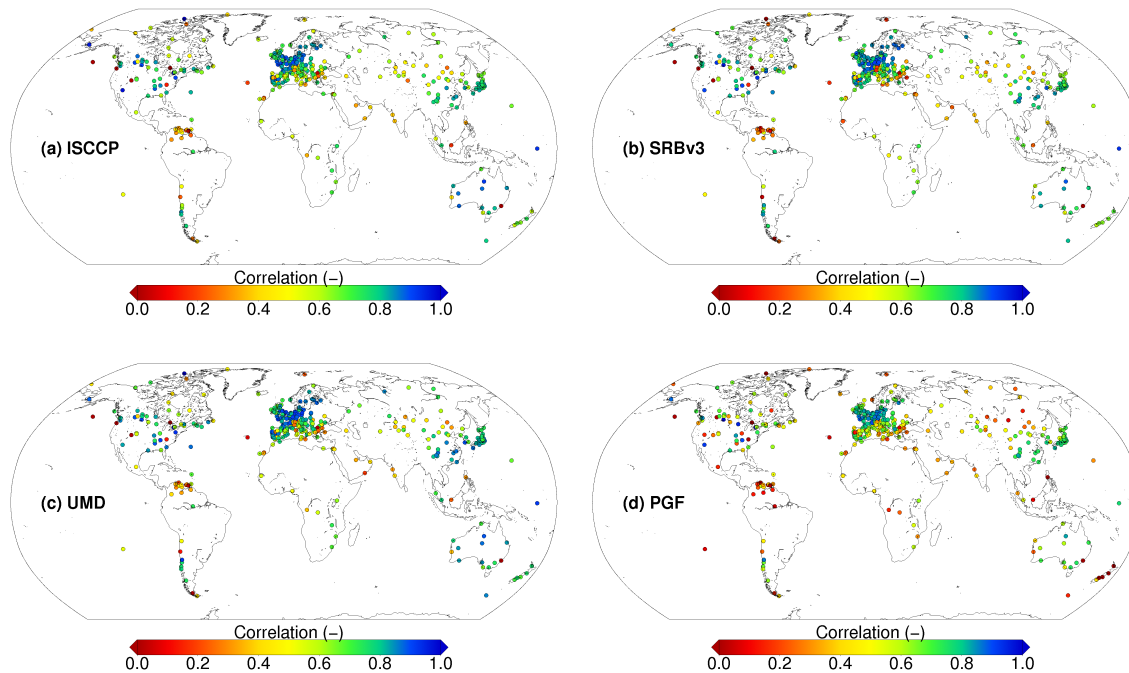
14

15

16

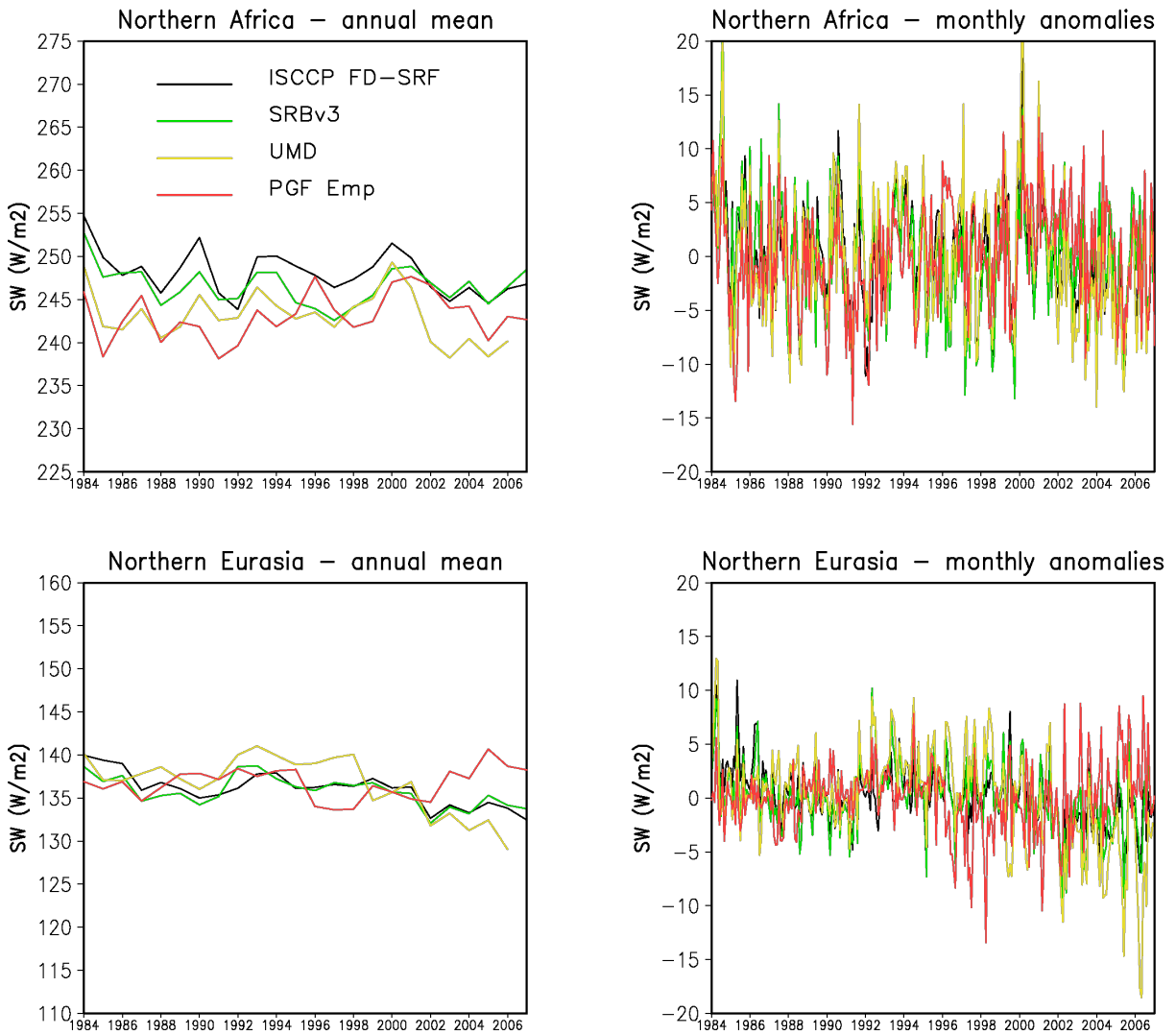


1
 2 **Figure S7.** Mean bias in downward surface solar radiation (dataset minus GEBA) for the three
 3 satellite datasets (a-c) and the empirical dataset (d). Biases are calculated for time periods with
 4 available stations data between 1984-2007. The number of records varies between GEBA
 5 stations, but a station is only used when a minimum of 10 years of data are available.



6
 7 **Figure S8.** As Figure S7, but for the correlation between the GEBA station data and the three
 8 satellite-based datasets (a-c) and the empirical dataset (d).

1



2
3
4
5

Figure S9. Regional average time series of downward surface solar radiation for (left) annual means and (right) monthly anomalies. Regions are as defined in the manuscript (see Figure 1).

1 ***Precipitation***

2 We estimate uncertainties in precipitation by evaluating three global precipitation datasets
3 (Table S4). These datasets are based on gauge measurements that are interpolated to a grid, and
4 in the case of the GPCP dataset merged with satellite estimates. The datasets differ in the set of
5 gauges that they use and the methods for quality-controlling the data and interpolating to a grid.
6 The differences among datasets are shown in Figure S10 in terms of the global land averaged
7 time series and the number of gauges contributing to each dataset. Figure S11 shows the time
8 series averaged over the focus regions.

9

10 *i) University of Delaware (UDel)*

11 This dataset is mainly based on station measurements from the quality-controlled monthly values
12 from the Global Historical Climatology Network (GHCN2) database, but is merged with data
13 from other global and regional datasets, with between 4100 to 22000 stations used globally each
14 year. No adjustment is made for raingauge undercatch. Station values were interpolated to 0.5-
15 degree resolution using climatologically aided interpolation (CAI) (Willmott and Robeson,
16 1995), which uses a background climatology taken from Legates and Willmott (1990). The
17 climatology is used to calculate differences at each station, which were then interpolated to the
18 grid and added back to the gridded climatology. Interpolation was done using a spherical version
19 of Shepard's algorithm, which employs an enhanced distance-weighting method (Shepard, 1968;
20 Willmott et al., 1985).

21

22

1 *ii) Climatic Research Unit (CRU)*

2 The CRU (V3.2) data (Harris et al., 2014) are based on CLIMAT records and Monthly Climatic
3 Data for the World (MCDW) obtained from the World Meteorological Organization (WMO) via
4 the US National Climatic Data Center (NCDC) with the number of stations included varying
5 from year to year with a maximum of about 2800. These are supplemented or replaced in some
6 cases by regional quality-controlled datasets where available. A similar method to the U.
7 Delaware dataset is used to produce gridded anomalies, but using percentages. Interpolation is
8 based on correlation decay distances, which is about 450km for precipitation and using
9 climatology where no nearby stations are available. Triangular linear interpolation is used to grid
10 the anomalies. Comparisons with the Global Precipitation Climatology Centre (GPCC; Schneider
11 et al., 2013) V5 shows a mean regional correlation of 0.89 with differences greater since the late
12 1990s in Alaska, Central America, and all African regions.

13

14 *iii) Global Precipitation Climatology Project (GPCP)*

15 The GPCP dataset (Adler et al., 2003; Huffman et al., 2009) merges satellite precipitation
16 retrievals with gauge climatology. Passive microwave estimates from the Special Sensor
17 Microwave/Imager (SSM/I) and Special Sensor Microwave Imager/Sounder (SSMIS) and
18 infrared (IR) precipitation estimates from primarily U.S., European and Japanese geostationary
19 satellites and secondarily from NOAA-series polar-orbiting satellites. Precipitation estimates are
20 also used from the Atmospheric Infrared Sounder (AIRS) data from the NASA Aqua, and
21 Television Infrared Observation Satellite Program (TIROS) Operational Vertical Sounder
22 (TOVS) and Outgoing Longwave Radiation (OLR) Precipitation Index (OPI) data. These
23 estimates are combined with the Global Precipitation Climatology Centre (GPCC) climatology to

1 provide a 2.5-degree gridded dataset. We interpolated the data to 0.5-degree for the CASA
2 simulations.

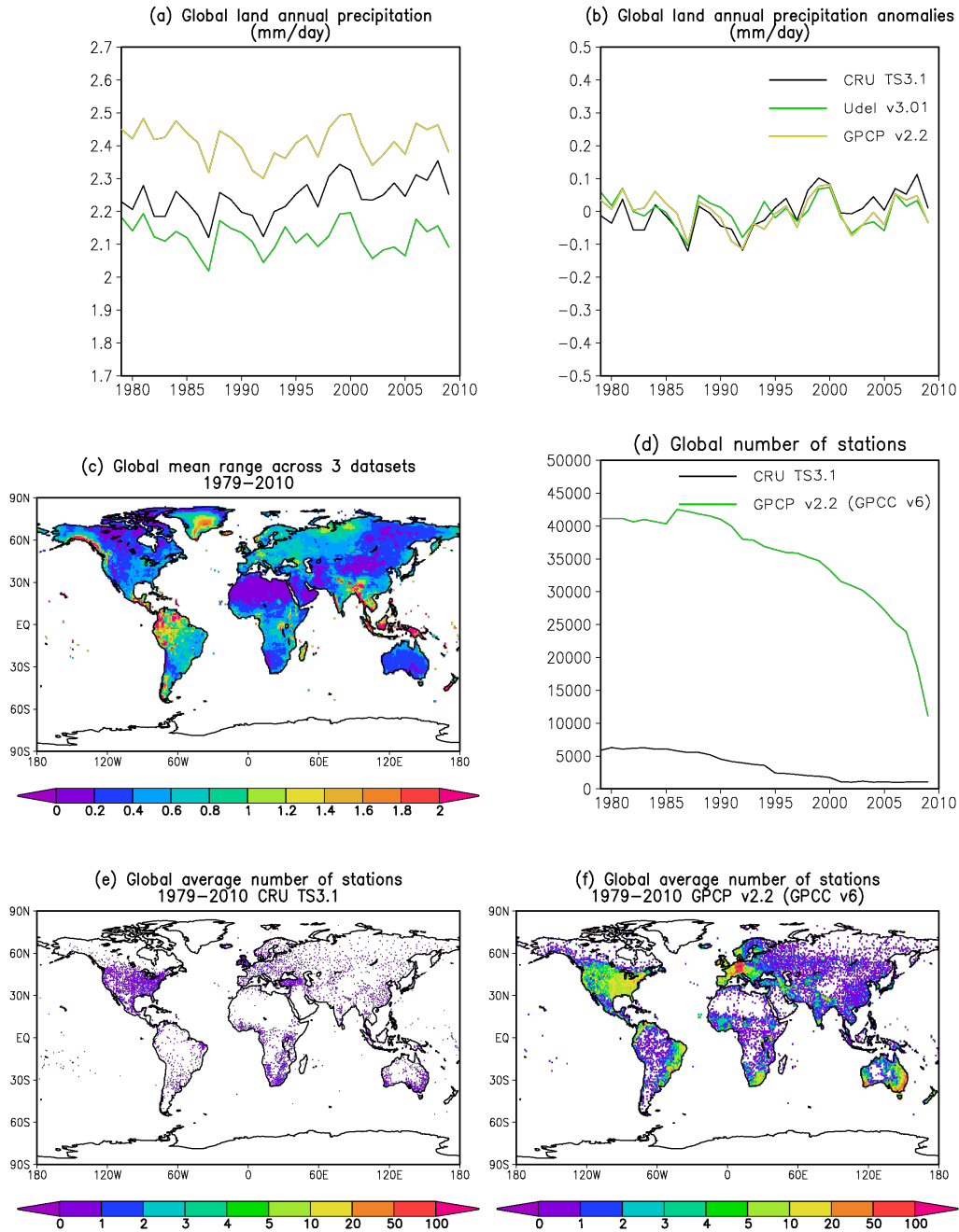
3

4 *iv) Comparison of precipitation datasets*

5 Figure S10 compares the three precipitation datasets in terms of global land time series of annual
6 mean and anomalies, and the number of contributing stations. The GPCP dataset is higher
7 globally than the other two datasets, which is partly because it adjusts for gauge undercatch,
8 which mainly increases values in wintertime over high latitudes (Figure S10a). The anomalies
9 are well correlated globally with the CRU dataset tending to have a positive trend in recent years
10 (Figure S10b). Regionally the differences are highest across southeast Asia and the Indonesian
11 islands, central America, parts of northwestern South America and the Pacific northwest of North
12 America (Figure S10c), which aligns with the regions of lowest gauge density, particularly for
13 the CRU dataset (Figure S10e,f). For the GPCP dataset, the satellite precipitation estimates are
14 merged with the GPCC station analysis (Schneider et al., 2013) and so we show the station count
15 for the GPCC dataset. The number of stations used by the CRU dataset is about 10% of that used
16 by the GPCC since the 1980s (Figure S10d), although the GPCC station count is very dense in a
17 few countries and the CRU stations tend to have long term records and therefore the CRU
18 datasets may be more temporally homogeneous. The station count for the UDel dataset is not
19 available but ranges between 4100 and 22000 stations per year and we assume that this is
20 somewhere between the GPCC and CRU station counts. The number of stations contributing to
21 each dataset has declined rapidly since the 1980s, and this has increased the differences between
22 the datasets relative to the period of highest densities (1960s-1970s; not shown). Regionally the
23 datasets are

24

1



2

3

4

5

6

7

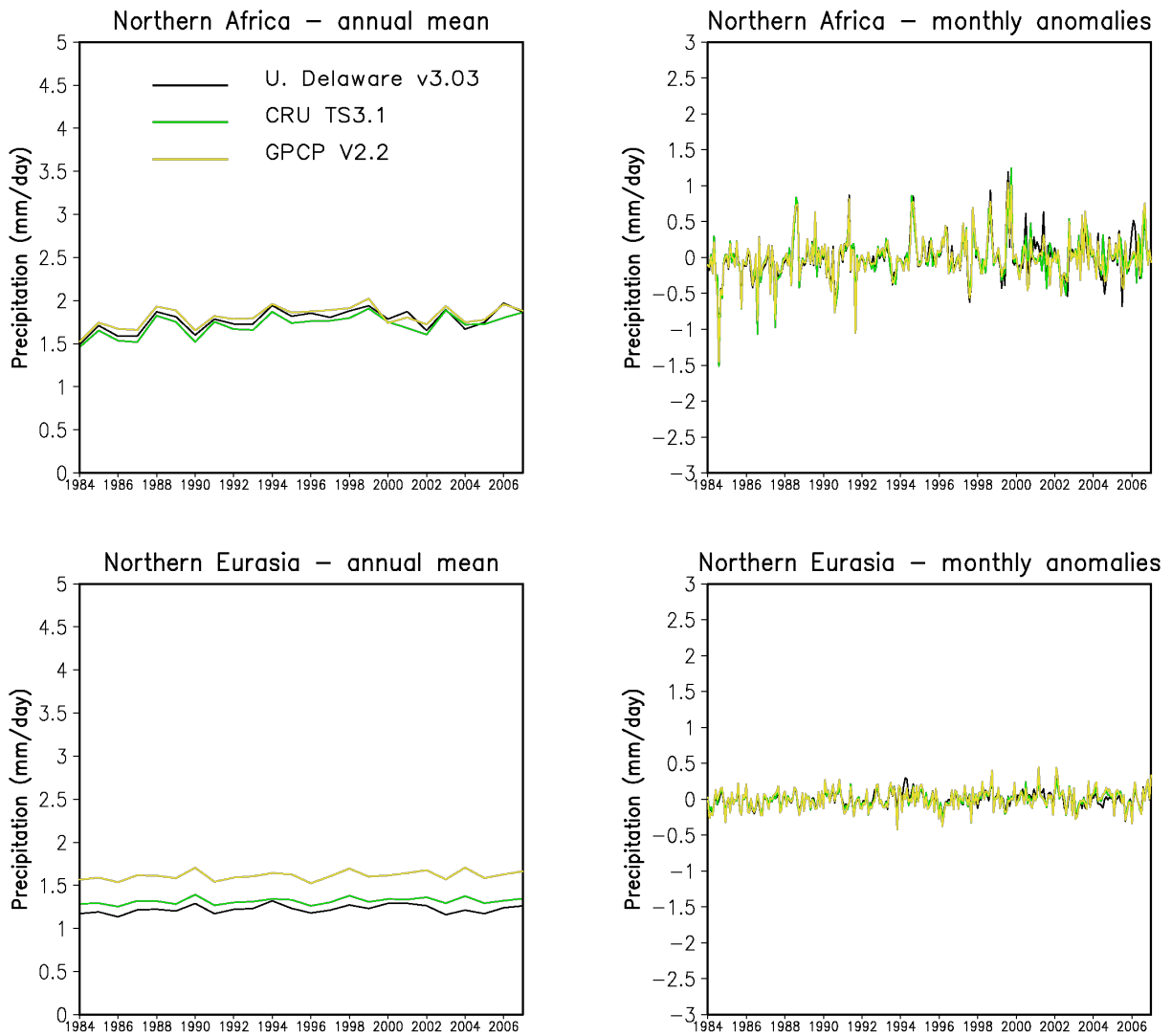
8

9

10

Figure S10. (a) Time series of annual mean precipitation (mm/day) averaged over land areas excluding Antarctica for the three precipitation datasets. (b) As (a) but for annual anomalies relative to 1979-2010. (c) Mean range in annual precipitation across the three datasets (mm/day). (d) Number of stations that contributed to the datasets. The GPCP datasets] is merged with station estimates from the GPCC dataset. No information is available on the number of stations for the UDel dataset. (e) Global distribution of the average number of stations for CRU TS3.1 for 1979-2010. (f) As (e) but for the GPCP v2.2 (based on GPCC v6).

- 1 very similar (Figure S11) with a slight divergence by the CRU dataset in recent years and higher
- 2 values in the GPCP in northern Eurasia because of the gauge undercatch correction.



3
4 **Figure S11.** Regional average time series of precipitation for (left) annual means and (right)
5 monthly anomalies. Regions are as defined in the main manuscript (see Fig. 1).
6
7

1 Supplement References

- 2 Adler, R.F., G.J. Huffman, A. Chang, R. Ferraro, P. Xie, J. Janowiak, B. Rudolf, U. Schneider, S.
3 Curtis, D. Bolvin, A. Gruber, J. Susskind, P. Arkin, E. Nelkin 2003: The Version 2 Global
4 Precipitation Climatology Project (GPCP) Monthly Precipitation Analysis (1979-Present). *J.*
5 *Hydrometeor.*, 4,1147-1167.
- 6 Enfield, D.B., A.M. Mestas-Nunez, and P.J. Trimble (2001) The Atlantic Multidecadal
7 Oscillation and its relationship to rainfall and river flows in the continental U.S., *Geophys.*
8 *Res. Lett.*, 28: 2077-2080.
- 9 Evan, A.T, A.K. Heidinger and D.J. Vimont (2007) Arguments against a physical long-term
10 trend in global ISCCP cloud amounts. *Geophys. Res. Lett.* 34, L04701.
- 11 Gilgen, H. and A. Ohmura (1999) The Global Energy Balance Archive (GEBA). *Bull. Am. Met.*
12 *Soc.*, 80, 831-850.
- 13 Harris, I., Jones, P.D., Osborn, T.J. and Lister, D.H. (2014), Updated high-resolution grids of
14 monthly climatic observations – the CRU TS3.10 Dataset. *Int. J. Climatol.*, 34: 623–642.
- 15 Hoerling, M.J., J. Hurrell, J. Eischeid, and A. Phillips (2006) Detection and attribution of 20th
16 century Northern and Southern African rainfall change. *J. Clim.* 19, 3989–4008.
- 17 Huffman, G.J, R.F. Adler, D.T. Bolvin, and G. Gu (2009) Improving the Global Precipitation
18 Record: GPCP Version 2.1. *Geophys. Res. Lett.*, 36, L17808.
- 19 Hurrell, J.W. (1995) Decadal trends in the North Atlantic oscillation regional temperatures and
20 precipitation. *Science* 269, 676–679.
- 21 Kalnay, E., and Coauthors, (1996) The NCEP/NCAR 40-Year Reanalysis Project. *Bull. Amer.*
22 *Meteor. Soc.*, 77, 437–471.
- 23 Kim Y, J.S. Kimball, K. Zhang and K.C. McDonald (2012) Satellite detection of increasing
24 Northern Hemisphere non-frozen seasons from 1979 to 2008: implications for regional
25 vegetation growth. *Remote Sens. Environ.* 121 472–87.
- 26 Legates, D. R. and C. J. Willmott (1990). Mean seasonal and spatial variability in gauge-
27 corrected, global precipitation. *International Journal of Climatology*, 10, 111-127.
- 28 Le Quéré , C., et al. (2009) Trends in the sources and sinks of carbon dioxide, *Nat. Geosci.* 2,
29 831–836.
- 30 Ma, Y., and R. T. Pinker (2012), Modeling shortwave radiative fluxes from satellites, *J.*
31 *Geophys. Res.*, 117, D23202.
- 32 Schneider, U. et al (2013): GPCP's new land surface precipitation climatology based on quality-
33 controlled in situ data and its role in quantifying the global water cycle. *Theoretical and*
34 *Applied Climatology* <http://dx.doi.org/10.1007/s00704-013-0860-x>
- 35 Sheffield, J., G. Goteti, and E.F. Wood (2006) Development of a 50-yr high-resolution global
36 dataset of meteorological forcings for land surface modeling, *J. Climate*, 19, 3088-3111.
- 37 Shepard, D. (1968). A two-dimensional interpolation function for irregularly-spaced data.
38 *Proceedings, 1968 ACM National Conference*, 517-523.
- 39 Stackhouse, Jr., P.W., et al. (2011) The NASA/GEWEX Surface Radiation Budget Release 3.0:
40 24.5-Year Dataset. *GEWEX News*, 21, 10-12.
- 41 Thompson, D.W.J. & J.M. Wallace (1998) The Arctic oscillation signature in the wintertime
42 geopotential height and temperature fields. *Geophys. Res. Lett.* 25, 1297–1300.
- 43 Willmott, C.J. and S.M. Robeson (1995). Climatologically aided interpolation (CAI) of
44 terrestrial air temperature. *International Journal of Climatology*, 15(2), 221-229.

1 Willmott, C. J., C. M. Rowe and W. D. Philpot (1985). Small-scale climate maps: a sensitivity
2 analysis of some common assumptions associated with grid-point interpolation and
3 contouring. *American Cartographer*, 12, 5-16.

4 Willmott, C. J. and K. Matsuura (2012) Terrestrial Air Temperature and Precipitation: Monthly
5 and Annual Time Series (1900 - 2010),
6 [http://climate.geog.udel.edu/~climate/html_pages/Global2011/README.GlobalTsP2011.ht](http://climate.geog.udel.edu/~climate/html_pages/Global2011/README.GlobalTsP2011.html)
7 [ml](http://climate.geog.udel.edu/~climate/html_pages/Global2011/README.GlobalTsP2011.html).

8 Zhang, Y., et al. (2004), Calculation of radiative fluxes from the surface to top of atmosphere
9 based on ISCCP and other global data sets: Refinements of the radiative transfer model and
10 the input data. *J. Geophys. Res.*, 109, D19105.

11

12

13